Dalton Transactions

ROYAL SOCIETY OF CHEMISTRY

PAPER

View Article Online
View Journal | View Issue

Check for updates

Cite this: *Dalton Trans.*, 2024, **53**, 17083

Gradual spin crossover behavior encompasing room temperature in an iron(II) complex based on a heteroscorpionate ligand†

Oleksandr Ye. Horniichuk, Laure Vendier, Lionel Salmon * and Azzedine Bousseksou*

Received 6th August 2024,
Accepted 25th September 2024

DOI: 10.1039/d4dt02244k

rsc.li/dalton

In this paper, we report the synthesis of six novel triazole-based heteroscorpionate ligands based on heterocycle metathesis reactions and their iron(II) complexes. Single crystal structure analyses were performed, the spectroscopic and magnetic properties of the obtained complexes were studied and their spin crossover–structural relationships were compared to those obtained for their pyrazole-based analogues reported in the literature. In particular, the amino derivative complex bis[hydrobis(pyrazol-1-yl)(3-amino-1,2,4-triazol-1-yl)]iron(II) obtained by post-synthetic catalytic nitro-group reduction under pressure of hydrogen in an autoclave presents a scarce gradual spin crossover behavior at room temperature. The profile of the SCO curve can be explained by the presence of only relatively weak H bonds, spreading only in one dimension. Among the interesting spin transition behaviors observed for the different complexes, such stable, complete and gradual spin crossover at room temperature makes this neutral complex a good candidate for sublimation and future investigation as an active element notably for thermoreflectance-based surface microthermometry applications.

Introduction

The spin crossover (SCO) phenomenon refers to a change in the spin state of first-row transition metal complexes with central ion electronic configurations of d^4–d^7 induced by external stimuli that include temperature, pressure, light or magnetic field.[1–3] The phenomenon typically occurs in complexes with an octahedral ligand field and is most abundant for the electronic configuration d^6 where iron(II) complexes are prevalent examples. One of the objectives to better integrate these materials into devices for real applications is to develop (thin) films.[4,5] Over decades of research, various techniques to obtain such films have been developed, which include the Langmuir–Blodgett technique,[6,7] spin coating,[8,9] drop casting,[10] surface layer-by-layer assembly,[11,12] vacuum deposition,[13,14] *etc*.[4] The vast majority of applications involving thin films require high quality, purity and homogeneity of the film. To fulfil these criteria, thermal vacuum deposition serves as a powerful means.[13,15] Currently, only a limited number of SCO complexes are known to be capable of being deposited by this technique.[13–29] Such a limited range of spin crossover compounds suitable for vacuum deposition can be explained by the fact that the compound candidates for thermal vacuum evaporation should be prone to sublimation and thus meet certain criteria, such as relatively low molecular weight, charge neutrality, a discrete structure and the absence of solvent or other guest molecules in their crystal lattice. However, the cationic iron(III) complex $[Fe(pap)_2]ClO_4{\cdot}H_2O$ (pap = *N*-2-pyridylmethylidene-2-hydroxyphenylaminato) is the only exception to this rule.[20] Heteroleptic Fe^{II} complexes $[Fe(H_2B(pz)_2)_2phen]$, $[Fe(H_2B(pz)_2)_2bpy]$ (pz = pyrazol-1-yl; phen = 1,10-phenanthroline; and bpy = 2,2′-bipyridine) and some of their derivatives substituted at the phen or bpy cores and $[Fe(pypyr(CF_3)_2)_2phen]$ (pypyr = 2-(2′-pyridyl)pyrrolide) can undergo surface-induced fragmentation to $[FeL_2]$ or $[FeL]^+$ (L = $H_2B(pz)_2$ or pypyr respectively) and phen (bpy) on certain metallic substrates at monolayer and sub-monolayer coverages.[30–32] In contrast, homoleptic iron(II) complexes with scorpionate-type tripodal hydrotris(azol-1-yl)borate ligands[33] do not dissociate on surfaces and can represent a stable alternative to their heteroleptic counterparts.[34]

The majority of applications require materials that switch around or above room temperature with or without a hysteresis loop.[35] Among the sublimable SCO complexes, only a few are known to undergo spin crossover above room temperature in

LCC, CNRS and Université de Toulouse (UPS, INP), 205 Route de Narbonne, F-31077 Toulouse, France. E-mail: lionel.salmon@lcc-toulouse.fr

†Electronic supplementary information (ESI) available: NMR and IR spectra, X-ray diffraction data and magnetism and Mössbauer measurements. CCDC 2370860–2370867. For ESI and crystallographic data in CIF or other electronic format see DOI: https://doi.org/10.1039/d4dt02244k

both bulk and thin-film states; those include [Fe(pypyr(CF$_3$)$_2$)$_2$phen],[36] [Fe(HB(pz)$_3$)$_2$],[23,37] [Fe(HB(1,2,3-tz)$_3$)$_2$][25,38] and [Fe(HB(1,2,4-tz)$_3$)$_2$].[16,39] It is noteworthy that the latter three belong to the scorpionate family of complexes. The temperature of spin transition $T_{1/2}$ for Fe-pypyr thin films (~330 K) is nearly 60 K lower compared to the bulk substance (390 K), while the other three compounds show comparable SCO properties in bulk and thin film forms ($T_{1/2} \approx$ 393 K, 373 K and 335 K for the pyrazolyl, 1,2,3-triazolyl and 1,2,4-triazolyl derivatives, respectively). The properties of [Fe(HB(1,2,4-tz)$_3$)$_2$] thin films were investigated in the 20–200 nm thickness range. It was found that the considered films are of high quality and show unprecedented endurance towards thermal cycling withstanding over 10 million heating–cooling cycles while remaining intact.[24]

Such an outstanding stability of the films makes them appropriate materials to elaborate miscellaneous functional devices for photonics, molecular electronics, actuators, sensors and temperature damping.[24,40–44] In particular, thermometry based on thermoreflectance allows high thermal and temporal resolution and provides the possibility to perform both qualitative and quantitative measurements. Despite the advantages that an abrupt spin transition can offer for thermometry, it does not allow for continuous real-time temperature monitoring enabled by a gradual transition. The issue was addressed by the use of a coating of the SCO [Fe(HB(1,2,3-tz)$_3$)$_2$] complex.[25]

Recent work of several research groups has reported a potential extension to the family of sublimable spin crossover compounds switching their spin states above room temperature.[45–47] The reported compounds belong to the class of heteroscorpionates. Unlike common (homo)scorpionates, in heteroscorpionates the N-donor azol-1-yl rings are not identical.[33] Flötotto *et al.* have developed a synthetic path to access new iron(II) heteroscorpionates, which involves the exchange of the pyrazole ring for a 4-nitropyrazole in the initial [HB(pz)$_3$]$^-$ ligand driven by the difference in the pK_a of the heterocycles.[45] They have successfully demonstrated that by controlling the temperature and stoichiometry, it is possible to selectively substitute one to all three pyrazol-1-yl moieties in the anionic ligand with their nitro counterpart. Moreover, the susceptibility of the NO_2 group to reduction offers a route to post-modification of the complexes. Using the above-discussed reaction of pyrazole exchange with 3(5)-nitro- and 4-nitropyrazoles, Ma *et al.* have complemented the library of nitro- and amino-decorated iron(II) hydrotris(pyrazol-1-yl)borates.[46] They have shown that the occurrence of SCO behavior in the resulting complexes depends on steric and electronic factors determined by the substituent position of the pyrazole ring, its steric demands and electronic properties. Desrochers *et al.* used the reaction of heterocycle metathesis to replace one 3,5-dimethylpyrazole ring in the [HB(3,5-Me$_2$pz)$_3$]$^-$ ligand with benzotriazole (btz) to obtain the first ferrous heteroazolyl heteroscorpionate [Fe(HB(3,5-Me$_2$pz)$_2$(btz)$_2$)$_2$].[47] As synthesized, the substance constitutes a mixture of *cis*- and *trans*-isomers separable by column chromatography. Both isomers display spin state changes in the high temperature region ($T_{1/2} \approx$ 385 K for the *cis*-isomer and $T_{1/2} \approx$ 372 K for the *trans*-isomer).

Thus, a range of evaporable spin crossover complexes have been synthesized up to date; however, this domain of research is still on the rise and requires the development of new SCO coordination compounds and their thin-film materials. The present work concerns the synthesis of novel triazole-based heteroazolyl heteroscorpionate ligands and their iron(II) complexes. Their structure, physico-chemical properties and magnetic behavior were analyzed and compared to those obtained for their pyrazole-based analogues reported in the literature.

Experimental section

Techniques and methods

IR spectra were recorded on a PerkinElmer FT-IR Frontier MIR/FIR spectrometer, using a diamond ATR (Attenuated Total Reflection). NMR spectra were recorded with a Bruker Avance III 400 (400 MHz) at 298 K using deuterated solvents CD_3OD and CD_2Cl_2. The chemical shifts, δ, for ^{1}H, ^{13}C and ^{11}B NMR are expressed in ppm. ^{11}B NMR spectra were recorded using $BF_3{\cdot}OEt_2$ as an external reference. Elemental analyses (for C, H and N) were performed using a PerkinElmer 2400 Series II instrument. Single-crystal X-ray diffraction analysis for ^{n}Bu$_4$N**L^1** was performed on a Rigaku Gemini Ultra diffractometer using graphite-monochromated Cu-Kα radiation (λ = 1.54184 Å). The single crystal of the *trans*-isomer complex **3** was analyzed on a Bruker Kappa Apex II diffractometer equipped with a 30 W air-cooled microfocus source using MoKα radiation (λ = 0.71073 Å). Suitable single crystals of the *cis*-isomer complexes **3** and **5** were analyzed using a Rigaku XtaLAB Synergy Dualflex diffractometer equipped with a PhotonJet X-ray source (Cu, λ = 1.54184 Å). Data were collected between 100 and 393 K; all diffractometers are equipped with an Oxford Instrument Cooler Device. The structures have been solved using the new dual-space algorithm program SHELXT[48] and refined by means of least-squares procedures either using the SHELXL-2018 [48] program included in the software package WinGX[49] version 1.639 or with the aid of the program CRYSTALS.[50] The atomic scattering factors were taken from the International Tables for X-Ray Crystallography.[51] Hydrogen atoms were placed geometrically and refined using a riding model. All non-hydrogen atoms were anisotropically refined. Ellipsoid plots in the figures of the Crystallography section were generated using ORTEP-3 software.[52] The crystal structures have been deposited at the Cambridge Crystallographic Data Centre and allocated the deposition numbers CCDC 2370860–2370867.† X-ray powder diffractograms for complexes **4** and **6** were recorded on capillaries, on a Rigaku Smartlab Powder Diffractometer using a Cu source ($\lambda_{K\alpha1}$ = 1.54056 Å) and a high energy linear detector (D Tex Ultra 250 from Rigaku). CCDC 2370860–2370867.† The diffractometer was used in a theta/theta configuration with multilayer mirror optics (CBO series for Smartlab). Data were recorded with 2θ between 5 and 70° or 5 and 50° (step: 0.01° or 0.02°). Variable-

temperature magnetic susceptibility data for complexes **2** and **3** were obtained in the 4–300 K range, at cooling and heating rates of 2 K min^{-1} under a field of 1 kOe using a Quantum Design MPMS magnetometer. For complexes **4–7**, the data were acquired in the 4–400 K range on a Quantum Design MPMS3 SQUID magnetometer using the same parameters. ^{57}Fe Mössbauer spectra were recorded using a conventional constant-acceleration-type spectrometer equipped with a 50 mCi ^{57}Co source and a liquid nitrogen cryostat. Least-squares fitting of the Mössbauer spectra was carried out with the assumption of Lorentzian line shapes using Recoil software.[53]

Syntheses of ligands and complexes

If not specified otherwise, all reactants and reagents used in this study were procured from commercial suppliers and employed as received. A solvent purification system PS-MD-5 (Inert Corporation, USA) was used to provide dry air-free dichloromethane for the synthesis of iron(II) complexes **1–4**. The synthesis of **KTp** was performed according to the procedure developed by Trofimenko,[54] with modifications specified in the respective protocol below. ^{n}Bu$_4$NTp was synthesized according to the literature protocol.[55] All the ligands are poorly soluble in water, but soluble in alcohols, DCM and aprotic polar organic solvents, in particular, tetrahydrofuran (THF), acetonitrile and acetone.

Potassium hydrotris(pyrazol-1-yl)borate (KTp). The stepwise heating of a KBH_4 (2.07 g, 38 mmol) and pyrazole (10.39 g, 153 mmol) powder mixture to 195 °C was performed according to the protocol reported by Trofimenko.[54] After around 3 h of heating under vigorous stirring of the formed melt, the hydrogen evolution ceased. Then the mixture was cooled down to 150 °C and stirred overnight at this temperature. Afterwards, the temperature was raised to 195 °C once again and the melt was vigorously stirred for another 3 h, after which it was cooled down to 65 °C. Once this temperature was reached, 30 ml of hot diethyl ether was added and the resulting mixture was stirred for 5 min. The white precipitate formed was filtered, thoroughly washed with hot ether and dried in air to yield 7.50 g of the product appearing as a white powder. Yield: 78%. ^{1}H NMR (400 MHz, CD_3OD) δ 7.51 (d, J = 2.0 Hz, 3H), 7.15 (d, J = 2.0 Hz, 3H), 6.15 (t, J = 2.0 Hz, 3H); ^{11}B NMR (128 MHz, CD_3OD) δ −1.15 (d).

***n*-Tetrabutylammonium (3-nitro-1,2,4-triazol-1-yl)di(pyrazol-1-yl)hydroborate (^{n}Bu$_4$NL^1).** ^{n}Bu$_4$NTp (1.99 g, 4.39 mmol) and 3-nitro-1,2,4-triazole (0.50 g, 4.39 mmol) powders were mixed in a Schlenk tube equipped with a magnetic stirring bar and an air-cooled distillation condenser connected to a receiving flask. Then, reduced pressure in the setup was created using a vacuum pump. Afterwards, the setup was sealed under reduced pressure. The bottom of the Schlenk tube was immersed in an oil bath resting on a magnetic stirring and heating plate. Then, the reaction mixture was heated at 100 °C under stirring for 2 h. The solid mixture started to melt at 90 °C. Condensation of crystalline pyrazole on the cooler parts of the tube walls was observed under these conditions. The deposited pyrazole was distilled under vacuum every 1 h. A crude oily product is obtained as a result. The temperature was reduced then to 75 °C, and water (20 mL) was added to the crude product and the obtained mixture was stirred at this temperature for 5 min. Then the stirring was stopped and the mixture was cooled to room temperature. The oily product collected at the bottom of the tube and on the walls. The aqueous phase was removed by decantation and the residue was dried in a vacuum, yielding 1.68 g of the product as a clear yellow oil. Yield: 76%. Single crystals, suitable for X-ray diffraction, formed in the crude product left overnight at room temperature. IR (neat, cm^{-1}): 2963m, 2937w, 2877w, 2460w (ν(B–H)), 1526m, 1540m, 1492s, 1474s, 1384vs, 1298vs, 1165s, 1109m, 1080m, 1030m; ^{1}H NMR (400 MHz, CD_2Cl_2) δ 7.93 (s, 1H), 7.56–7.54 (m, 4H), 6.18 (t, J = 2.2, 2H), 4.79 (q, J_{HB} = 144 Hz, 1H), 3.10–3.01 (m, 8H), 1.62–1.49 (m, 8H), 1.43–1.29 (m, 8H), 0.97 (t, J = 7.3 Hz, 12H); ^{13}C NMR (101 MHz, CD_2Cl_2) δ 152.39, 149.11, 140.39, 134.16, 104.26, 59.05, 24.14, 19.98, 13.69; ^{11}B NMR (128 MHz, CD_2Cl_2) δ −1.57 (d); $C_{24}H_{44}BN_9O_2$ (M = 501.49). Anal. calc.: C, 57.48; H, 8.84; N, 25.14%. Found: C, 57.39; H, 8.88; N, 25.27%.

***n*-Tetrabutylammonium bis(3-nitro-1,2,4-triazol-1-yl)(pyrazol-1-yl)hydroborate (^{n}Bu$_4$NL^2).** The same setup as in the case of ^{n}Bu$_4$NL^2 was used and the procedure was similar, with differences in stoichiometry and temperature. Thus, ^{n}Bu$_4$NTp (1.00 g, 2.20 mmol) and 3-nitro-1,2,4-triazole (0.50 g, 4.39 mmol) were heated at 130 °C under stirring for 3 h. Pyrazole was distilled off every 1 h. The purification step of stirring the crude product in water was carried out as described in the previous protocol. The product appeared as a viscous clear dark-yellow oil. 1 g. Yield: 83%. IR (neat, cm^{-1}): 2964m, 2936w, 2876w, 2472w (ν(B–H)), 1541s, 1494s, 1413m, 1384m, 1297vs, 1167s, 1104m, 1024m; ^{1}H NMR (400 MHz, CD_2Cl_2) δ 8.20 (s, 2H), 7.72 (d, J = 2.2 Hz, 1H), 7.65 (d, J = 2.2 Hz, 1H), 6.26 (d, J = 2.2 Hz, 1H), 4.79 (q, J_{HB} = 143 Hz, 1H), 3.21–3.05 (m, 8H), 1.62 (p, J = 7.3 Hz, 8H), 1.38 (h, J = 7.3 Hz, 8H), 0.97 (t, J = 7.3 Hz, 12H); ^{13}C NMR (101 MHz, CD_2Cl_2) δ 149.54, 148.35, 141.64, 135.34, 105.10, 59.30, 24.15, 20.02, 13.63; ^{11}B NMR (128 MHz, CD_2Cl_2) δ −2.30 (d); $C_{23}H_{42}BN_{11}O_4$ (M = 547.47). Anal. calc.: C, 50.46; H, 7.73; N, 28.14%. Found: C, 50.47; H, 7.88; N, 28.35%.

The CN-bearing derivatives of **L^3** and **L^4** were obtained following the same protocols as for their nitro-featured counterparts using 3-cyano-1,2,4-triazole instead of 3-nitro-1,2,4-triazole.

***n*-Tetrabutylammonium (3-cyano-1,2,4-triazol-1-yl)di(-pyrazol-1-yl)hydroborate (^{n}Bu$_4$NL^3).** Clear colorless oily product. Yield: 69%. IR (neat, cm^{-1}): 2963m, 2937w, 2876w, 2455w (ν(B–H)), 2245w (ν(C≡N)), 1500w, 1470s, 1413w, 1384s, 1291s, 1161vs, 1107vs, 1096vs, 1034vs; ^{1}H NMR (400 MHz, CD_2Cl_2) δ 7.99 (s, 1H), 7.52 (d, J = 2.1 Hz, 2H), 7.50 (d, J = 2.1 Hz, 2H), 6.16 (t, J = 2.1, 2H), 4.78 (q, J_{HB} = 138 Hz, 1H), 3.10–2.93 (m, 8H), 1.61–1.49 (m, 8H), 1.44–1.30 (m, 8H), 0.99 (t, J = 7.3 Hz, 12H); ^{13}C NMR (101 MHz, CD_2Cl_2) δ 149.35, 140.28, 139.29, 134.12, 114.61, 104.20, 59.10, 24.19, 20.03, 13.72. ^{11}B NMR (128 MHz, CD_2Cl_2) δ −1.66 (d); $C_{25}H_{44}BN_9$ (M = 481.50). Anal. calc.: C, 62.36; H, 9.21; N, 26.18%. Found: C, 62.70; H, 9.52; N, 26.09%.

***n*-Tetrabutylammonium bis(3-cyano-1,2,4-triazol-1-yl)(pyrazol-1-yl)hydroborate (^{n}Bu$_4$NL^4).** Colorless clear oil. Yield: 94%. IR (neat, cm^{-1}): 2964m, 2937w, 2877w, 2476w (ν(B–H)), 2247w (ν(C≡N)), 1506w, 1470s, 1415w, 1386m, 1315s, 1166vs, 1104s, 1030vs; ^{1}H NMR (400 MHz, CD_2Cl_2) δ 8.19 (s, 2H), 7.65 (d, J = 2.2 Hz, 1H), 7.60 (d, J = 2.2 Hz, 1H), 6.23 (t, J = 2.2 Hz, 1H), 4.77 (q, J_{HB} = 142 Hz, 1H), 3.15–3.03 (m, 8H), 1.67–1.52 (m, 8H), 1.45–1.31 (m, 8H), 0.98 (t, J = 7.3 Hz, 12H); ^{13}C NMR (101 MHz, CD_2Cl_2) δ 149.58, 141.27, 139.81, 134.96, 114.22, 104.91, 59.32, 24.17, 20.02, 13.66; ^{11}B NMR (128 MHz, CD_2Cl_2) δ −2.59 (d); $C_{25}H_{42}BN_{11}$ (M = 507.50). Anal. calc.: C, 59.17; H, 8.34; N, 30.36%. Found: C, 59.40; H, 8.33; N, 30.40%.

The synthesis of the iron(II) complexes **2–5** was carried out under an argon atmosphere using common anaerobic Schlenk techniques. The reduction of the nitro-derived complexes **2** and **3** was conducted in a 50 ml autoclave (Autoclave-Maxitech, France) pressurized with hydrogen gas. Synthetic procedures to access iron(II) complexes with ligands **L^1–L^4** were conducted as follows.

Bis[hydrobis(pyrazol-1-yl)(3-nitro-1,2,4-triazol-1-yl)]iron(II) [Fe(L^1)$_2$] (1). To a solution of ^{n}Bu$_4$NL^1 (1.60 g, 3.20 mmol) in dry air-free DCM (95 mL), $FeCl_2{\cdot}4H_2O$ (0.32 g, 1.60 mmol) was added under argon. The solution gradually turned dark pink following the $FeCl_2$ consumption. After vigorous stirring for 1 h at room temperature, the solvent was removed under reduced pressure, and the remaining residue was suspended in water (60 mL). The formed precipitate was filtered, thoroughly washed with water and dried in air to afford 0.76 g of a brick-red powder of the product. Yield: 83%. The compound is insoluble in water, poorly soluble in alcohols, and soluble in DCM, THF and acetone. IR (neat, cm^{-1}): 3116w, 2487w (ν(B–H)), 1552m, 1501s, 1402m, 1307s, 1167s, 1050s; $C_{16}H_{16}B_2FeN_{16}O_4$ (M = 573.88). Anal. calc.: C, 33.49; H, 2.81; N, 39.05%. Found: C, 33.20; H, 2.61; N, 38.88%.

Bis[hydrobis(3-nitro-1,2,4-triazol-1-yl)(pyrazol-1-yl)]iron(II) [Fe(L^2)$_2$] (2). The synthetic procedure for this compound is the same as for **1**; however, the isolation of the product was carried out differently. Thus, to a solution of ^{n}Bu$_4$NL^2 (0.88 g, 1.61 mmol) in dry air-free DCM (50 mL), $FeCl_2{\cdot}4H_2O$ (0.16 g, 0.80 mmol) was added under argon. After vigorous stirring for 1 h at room temperature, the solvent was removed under vacuum. The residue was suspended in a minimal amount of ethanol. The formed precipitate was filtered, washed with cold EtOH and air-dried to afford 0.35 g of product as a yellow powder. Its solubility properties are similar to those of **2**; however, the compound is more readily soluble in alcohols. Yield: 64%. IR (neat, cm^{-1}): 3144w, 2517w (ν(B–H)), 1554m, 1501s, 1421m, 1311vs, 1173s, 1046m; $C_{14}H_{12}B_2FeN_{20}O_8$ (M = 665.85). Anal. calc.: C, 25.25; H, 1.82; N, 42.07%. Found: C, 25.41; H, 1.86; N, 41.95%.

Bis[hydrobis(pyrazol-1-yl)(3-cyano-1,2,4-triazol-1-yl)]iron(II) [Fe(L^3)$_2$] (3). The synthesis and work-up procedure were the same as for **1**. The substance appears as a brick-red powder. Yield: 65%. The solubility of the compound is similar to that of complex **2**. Single crystals suitable for X-ray diffraction were obtained by slow solvent evaporation from a saturated DCM solution. IR (neat, cm^{-1}): 3114w, 2511w (ν(B–H)), 2248w (ν(C≡N)), 1501w, 1469w, 1406m, 1315m, 1220m, 1171m, 1112m, 1049m, 755s, 713vs; $C_{18}H_{16}B_2FeN_{16}$ (M = 533.90). Anal. calc.: C, 40.49; H, 3.02; N, 41.98%. Found: C, 40.53; H, 2.95; N, 41.82%.

Bis[hydrobis(3-cyano-1,2,4-triazol-1-yl)(pyrazol-1-yl)]iron(II) [Fe(L^4)$_2$] (4). $FeCl_2{\cdot}4H_2O$ (0.31 g, 1.56 mmol) was added to a vigorously stirred solution of ^{n}Bu$_4$NL^4 (1.56 g, 3.07 mmol) in dry air-free DCM (75 mL). After 5 min of stirring, a bright red precipitate appeared. The mixture was stirred for 1 h. Afterwards, the precipitate was filtered. The formation of the precipitate continued in the filtrate; thus, the latter was concentrated and the precipitate was filtered. For further purification, the precipitates may be subjected to washing with minimal quantities of ethanol as in the case of **3**. Eventually, an additional quantity of product is accessible by evaporation of the second filtrate and treatment of the residue with ethanol, yielding 0.42 g (yield: 47%). The compound is insoluble in water, poorly soluble in DCM, and soluble in alcohols and acetone. IR (neat, cm^{-1}): 3126w, 2526w (ν(B–H)), 2251w (ν(C≡N)), 1505w, 1464w, 1405w, 1337m, 1317w, 1167m, 1109w, 1020m, 761s, 712vs; $C_{18}H_{12}B_2FeN_{20}$ (M = 585.90). Anal. calc.: C, 36.90; H, 2.06; N, 47.81%. Found: C, 36.40; H, 2.33; N, 47.49%.

Bis[hydrobis(pyrazol-1-yl)(3-amino-1,2,4-triazol-1-yl)]iron(II) [Fe(L^5)$_2$] (5). Compound **1** (0.36 g, 0.63 mmol) and Pd/C (11 mg) were placed in an autoclave. The charged autoclave was degassed. Then, methanol (18 mL) was added. The resulting stirred suspension was heated to 80 °C and hydrogenated at 15 bars for 22 h. After cooling to room temperature and depressurizing, the content of the autoclave was poured into methanol (460 mL), and the obtained suspension was heated to sub-reflux under stirring in order to dissolve the product. Afterwards, the mixture was filtered to remove the catalyst. The filtrate was concentrated until the formation of a precipitate. The latter was filtered, washed with cold methanol and air-dried to afford 0.23 g of a deep purple powder of the product. Yield: 71%. The complex is poorly soluble in methanol. Single crystals suitable for X-ray diffraction are obtained by slow evaporation of the saturated methanolic solution. IR (neat, cm^{-1}): 3474w, 3307w (ν_{as}(NH_2)), 3215w (ν_s(NH_2)), 3168w (NH_2), 2474w (ν(B–H)), 1634m, 1548s, 1505m, 1392m, 1302s, 1206s, 1166s, 1107s, 1045s, 1023s; $C_{16}H_{20}B_2FeN_{16}$ (M = 513.91). Anal. calc.: C, 37.39; H, 3.92; N, 43.61%. Found: C, 37.63; H, 3.57; N, 43.49%.

Bis[hydrobis(3-amino-1,2,4-triazol-1-yl)(pyrazol-1-yl)]iron(II) [Fe(L^6)$_2$] (6). A stirred suspension of **2** (0.29 g, 0.44 mmol) and Pd/C (10 mg) in methanol (20 mL) was heated at 80 °C and hydrogenated at 30 bars for 22 h. After the hydrogenation, the catalyst was filtered and the solvent was removed *in vacuo* to afford 0.22 g of the product as a dark green solid. Yield: 91%. The substance is soluble in alcohols. IR (neat, cm^{-1}): 3464w, 3324w (ν_{as}(NH_2)), 3210w (ν_s(NH_2)), 3114w (NH_2), 2470w (ν(B–H)), 1614m, 1538s, 1505m, 1417w, 1388w, 1304m, 1210w, 1166s, 1110m, 1055s, 1025s, 1012s; $C_{16}H_{20}B_2FeN_{16}$ (M = 513.91). Anal. calc.: C, 30.69; H, 4.05; N, 51.13%. Found: C, 30.45; H, 4.30; N, 51.26%.

Results and discussion

Inspiration to design new scorpionate ligands and their Fe^{II} complexes was based on the heterocycle metathesis reaction described in the literature,[45,46] where the authors obtained novel spin-crossover complexes by replacing pyrazole units in tris(pyrazol-1-yl)borate derivatives with nitropyrazoles, with the possibility of post-functionalization of the resulting complexes. Instead of nitropyrazoles, 1,2,4-triazoles substituted with an electron withdrawing group ($-NO_2$ and $-CN$) at position 3 were used in this work. Nitro-functionalized derivatives were successfully converted to amines. At first, potassium hydrotris(pyrazol-1-yl)borate (hereafter **KTp**) was synthesized following the protocol developed by Trofimenko,[54] with a slightly modified work-up procedure (see the Experimental part). Then, potassium cation in the product was exchanged for tetrabutylammonium ($^{n}Bu_4N^+$ or TBA) according to the procedure reported in ref. 55. Then, the resulting TBA derivative $^{n}Bu_4NTp$ was heated with 1 (2) equivalent(s) of an EWG-bearing 1,2,4-triazole to obtain mono(di)substituted products, as shown in Fig. 1. As electron-withdrawing groups, nitro-group and cyano-group were selected. Thus, commercially available 3-nitro-1,2,4-triazole and 3-cyano-1,2,4-triazole were used for the reaction of heterocycle exchange to afford the new heteroscorpionate ligands. The reactions between $^{n}Bu_4NTp$ and the triazole reactants were conducted without any solvent under static vacuum conditions to promote the pyrazole release. The degree of substitution of pyrazole moieties with triazole moieties was controlled through stoichiometry and temperature alike. Thus, to replace one pyrazole unit (n = 1, Fig. 1), heating the reaction mixture at 90 °C was sufficient for the reaction to proceed. The optimal temperature range for monosubstitution was set between 90 and 105 °C. The primary evidence of the reaction is the condensation of the eliminated pyrazole crystals on the walls of the reaction vessel. The latter can be distilled under dynamic vacuum and collected in a receiving flask. This allowed us to conveniently monitor the reaction completion by measuring the weight of the released pyrazole. To this purpose, the latter was distilled off from the reaction vessel every one hour, and the collected distillate was weighed. The majority of pyrazole was released in the first hour of the reaction. Heating the reaction mixture for an additional hour yielded the rest of pyrazole; the pyrazole release was quantitative. The formation of the disubstituted derivatives was possible *via* heating the stoichiometric mixture of reactants to 130 °C. After around 95% of pyrazole was eliminated, its release ceased, reaching a maximum after 3 h of heating. As in the case of analogous reactions with nitropyrazoles, heterocycle metathesis involving the above-mentioned triazole reactants leads to selective formation of the desired mono- and disubstituted products, which can be controlled through temperature and stoichiometry.

However, attempts at trisubstitution, requiring 3 equivalents of a triazole reactant and higher temperatures (about 150 °C), led to the formation of a mixture of products with different degrees of substitution and by-products that were formed, most probably, as a result of side reactions taking place at high temperatures. The separation of products in this mixture appeared to be challenging. The scope of the synthesized ligands is depicted in Chart 1.

In the literature,[45,46] the authors propose a heterocycle metathesis mechanism based on the considerations of HSAB theory, according to which more acidic nitropyrazoles (pK_a = 9.50–9.75), attacking the boron core, readily give their pyrrole-type protons to the more basic pyrazolyl moiety, which eliminates as a free pyrazole (pK_a = 14.21).[56] Given that the acidity of 1,2,4-triazole (pK_a = 9.89)[57] is close to that of nitropyrazoles, it was interesting to carry out this reaction with unsubstituted triazole. Though the synthetic conditions for mono- and disubstitution were the same as those in the case of the substituted triazoles, the reactions with pristine triazole did not provide the same selectivity and resulted in a mixture of products that are challenging to separate. Similar results were achieved, when a triazole bearing an electron-donating amino group at position 3 was used as the reactant in an attempt to synthesize directly an amino-functionalized heteroscorpionate ligand. Considering the electron density donation from the amino group to the aromatic core, the pK_a of 3-amino-1,2,4-triazole is expected to be higher than that of pristine triazole; consequently, such a result was expected. Consequently, these results point to the conclusion that the presence of EWG in the triazole precursor is crucial for heterocycle metathesis to

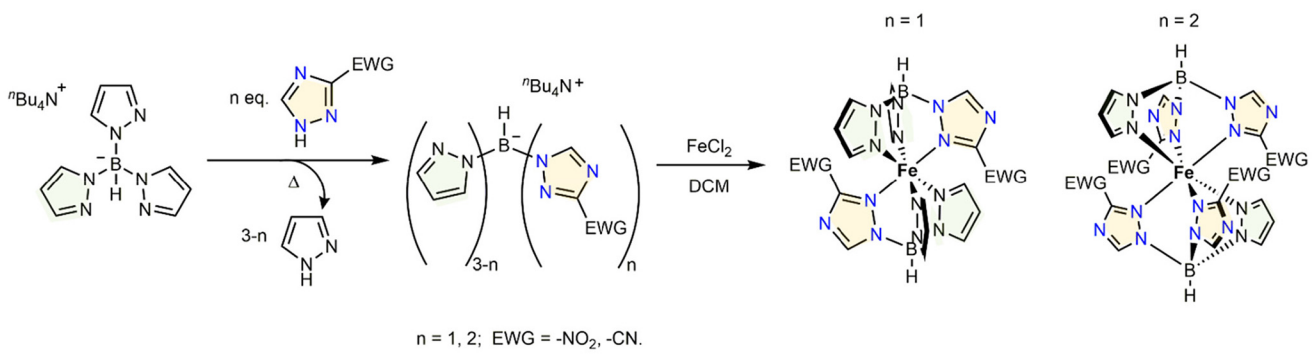

Fig. 1 Synthetic pathway to obtain triazole-based heteroazolyl heteroscorpionate ligands and their respective iron complexes.

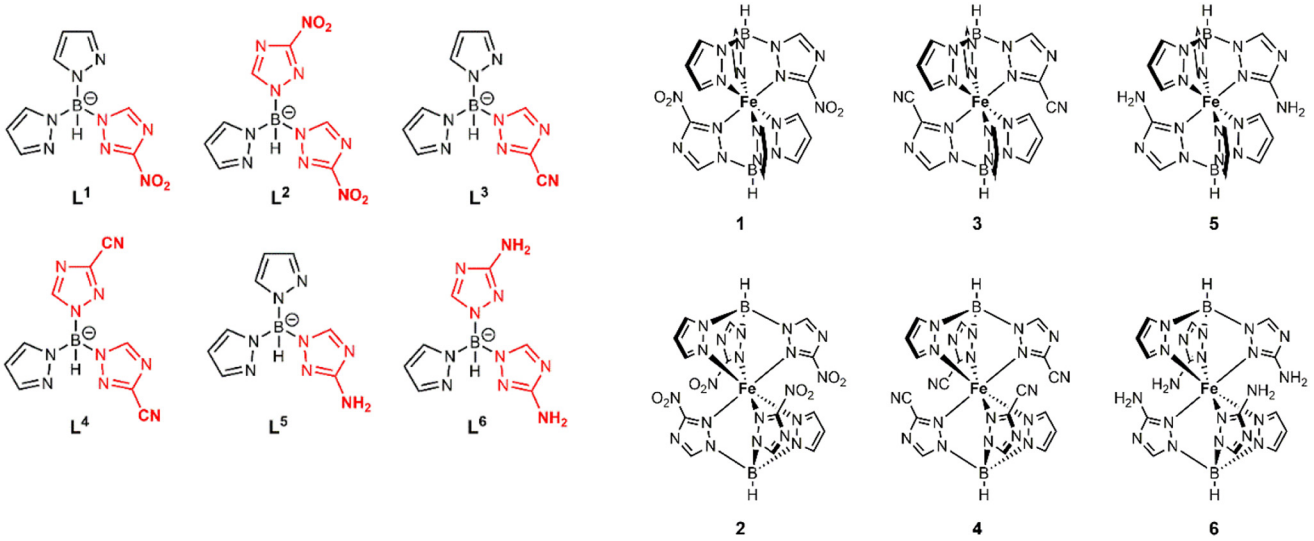

Chart 1 Scope of ligands (left) and complexes (right) synthesized in this work.

proceed as it provides a sufficient difference in pK_a between a triazole reactant and pyrazole, to shift the equilibrium towards the formation of the desired heteroscorpionates.

As the nitro group can be reduced to a primary amine, it was interesting to try to convert a nitro-derived ligand to an NH_2-bearing ligand that can be either directly coordinated to Fe^{II} or undergo functionalization of the amino group with the subsequent coordination of a modified ligand to the metal ion. For this purpose, the monosubstituted nitro-derived ligand $^nBu_4N\mathbf{L^1}$ was selected for reduction. The reduction reaction conditions were similar to those in the case of complexes reported in ref. 46, which involve the use of an organic reducing agent, a palladium catalyst, a protic solvent and microwave heating. In the present case, 1,4-cyclohexadiene was used as the reducing agent and palladium (5 wt%) on carbon was selected as the catalyst, while alcohols such as methanol or ethanol were used as solvents either pure or in an alcohol : toluene (3 : 1) mixture similar to those reported by Ma *et al.*[46] The first approach involved microwave heating (closed-vessel mode) of $^nBu_4N\mathbf{L^1}$ stirred methanolic solution at 120 °C for 5 minutes with an excess (6 equivalents) of 1,4-cyclohexadiene and in the presence (8 mol%) of Pd/C. Colorless crystals isolated after concentration of the obtained solution were analyzed by means of single crystal X-ray diffraction. Instead of the expected amino-derived hydroborate anion, the resulting crystal structure revealed an associate composed of a 3-amino-1,2,4-triazole anion binding three neutral pyrazole molecules *via* hydrogen bonding (see Fig. S1†). The negatively charged associate is compensated for by a TBA cation. Such a result indicates the degradation of the hydroborate anion, possibly due to solvolysis under the given conditions. The degradation is supported by NMR spectroscopy data. Solution ^{1}H NMR of an aliquot of the reaction mixture taken after 5 minutes of the reaction revealed two signals of free-pyrazole aromatic protons, while in the spectra of the scorpionate ligands, three signals are typically observed for pyrazole bound to boron (see the NMR spectrum in Fig. S2†). Changing the reaction conditions, *e.g.*, reducing the temperature together with increasing the time only retarded the degradation, but did not prevent it. Moreover, even after leaving the mixture of the reactants and the reagents overnight at room temperature with no stirring, degradation signs, such as the presence of the liberated pyrazole, could be detected. Varying the solvents did not have any notable impact on the reaction outcome. Such a chemical behavior is probably related to the presence of the palladium catalyst that in the protic solvent medium can promote the solvolysis of the hydroborate as is known in the case of borohydride.[58] Considering the fragility of the hydroborate anion, direct reduction of the nitro group in $\mathbf{L^1}$ and $\mathbf{L^2}$ to obtain $\mathbf{L^5}$ and $\mathbf{L^6}$ is probably not the most appropriate strategy. The reduction of the NO_2 group of the ligands in their iron(II) complexes (post-functionalization) is another approach, which is discussed further together with the synthesis of coordination compounds based on heteroscorpionate ligands.

The syntheses of iron(II) complexes with ligands $\mathbf{L^1}$–$\mathbf{L^4}$ were performed under an argon atmosphere in a degassed dichloromethane (DCM) solution starting from 2 equivalents of the respective ligand and 1 equivalent of $FeCl_2{\cdot}4H_2O$ (Fig. 1). Attempts to reduce complexes $[Fe(\mathbf{L^1})_2]$ under microwave conditions suggested by Ma *et al.*[46] and tried for uncoordinated $\mathbf{L^1}$ faced issues to obtain any reproducible results, which are related to the absence of possibility of control over the reaction outcome to obtain the desired product, resulting in fairly low yields (2–33%) of the reduction reaction product. Conversely, the classical technique of catalytic nitro-group reduction under pressure of hydrogen in an autoclave served as a reliable tool to convert NO_2-decorated substrates $[Fe(\mathbf{L^1})_2]$ and $[Fe(\mathbf{L^2})_2]$ into di- and tetraamines $[Fe(\mathbf{L^5})_2]$ and $[Fe(\mathbf{L^6})_2]$, respectively (Fig. 2). The reaction conditions were similar to those proposed by Flötotto *et al.* for the pyrazole-based counterpart.[45]

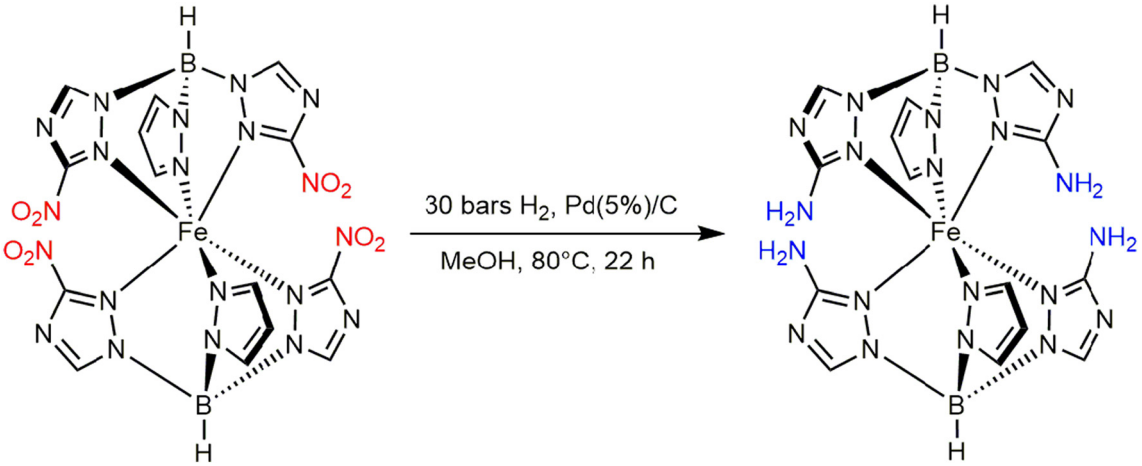

Fig. 2 Reduction of NO_2 groups in $[Fe(L^2)_2]$.

The synthetic procedures to access the ligands and their iron (II) complexes are provided in the Experimental part.

Spectroscopic characterization

The NMR spectra are presented in Fig. S3–S14.† In the proton NMR spectra of the ligands, the pyrazolyl moiety is characterized by three signals: two doublets at about 7.61 and 7.58 ppm (average chemical shift values) assigned to protons at positions 5 and 3 of the pyrazole ring, and a triplet at around 6.20 ppm corresponding to the proton at position 4. The triazolyl units bear only a single proton, the singlet signal of which appears at 7.93 (7.99) ppm for $\mathbf{L^1}$ ($\mathbf{L^3}$) and at 8.20 ppm in the case of $\mathbf{L^2}$ and $\mathbf{L^4}$. The integral intensity ratio of the triazole singlet to the pyrazole multiplets (s : d : d : t) is 1 : 2 : 2 : 2 for $\mathbf{L^1}$ and $\mathbf{L^3}$ and 2 : 1 : 1 : 1 for $\mathbf{L^2}$ and $\mathbf{L^4}$, which is in line with the expected structures of the respective heteroscorpionate anions. The ^{13}C NMR spectra of the ligands featuring nitro groups are characterized by the presence of four signals in the aromatic region of the spectra: one weak-field signal (~149 ppm) corresponding to the carbon nucleus at position 5 of the triazolyl moiety and three signals in the 140–105 ppm region from the pyrazole carbon nuclei. A large number of scans (>3000) in the NMR experiment may allow us to observe a weak signal of the carbon nucleus at position 3 of the triazole ring. For example, the signal can be observed for $\mathbf{L^1}$ at 152.39 ppm. In the spectra of the cyano-functionalized ligands, an extra signal of low intensity observed at 114.61 ppm for $\mathbf{L^3}$ and at 114.22 for $\mathbf{L^4}$ is assigned to the carbon nucleus of the CN group. Similar to the nitro derivatives, large scan numbers allow the observation of the position 3 aromatic carbon signal at 139.29 and 139.81 ppm for $\mathbf{L^3}$ and $\mathbf{L^4}$, respectively. The boron NMR spectra of all the ligands contain one doublet lying in the region from −2.59 to −1.57 ppm. The presence of the sole signal in the spectra as well as the multiplicity of the signal correlates well with the fact that the compounds contain only one type of boron nucleus directly linked to the proton nuclei of identical nuclear spin. The NMR spectra of the heteroscorpionate ligands recorded weeks or months after their synthesis reveal signs of stability issues in the ligands upon their storage under ambient conditions. Thus, an extra signal appears in the ^{11}B NMR spectra as a singlet at around 18 ppm, which is characteristic of boric acid and its esters.[59] Meanwhile in the proton NMR, an extra weak-field singlet appears in the 8.3–8.0 ppm region, most probably corresponding to the free triazole species. It should be noted that these impurity signals are also observed in the spectra of the crude products. Similar to the observations of $\mathbf{L^1}$ degradation under reduction conditions, the considered observations highlight the fact that heteroscorpionates have an inclination to degrade over time under ambient conditions, probably due to slow hydrolysis of the hydroborate species caused by moisture in the ambient air. This fact should be taken into account during the planning of ligand synthesis as well as the synthesis of complexes. Thus, practices such as using the ligands shortly after their synthesis or employing anaerobic techniques for preparation, handling and storage of the compounds can be applied to ensure substance purity and to minimize or avoid undesired degradation processes.

The IR spectra are presented in Fig. S15–S24.† A characteristic vibration band for boron-based scorpionate ligands is the B–H stretch appearing well apart from other bands within the 2460–2526 cm^{-1} range in the case of the considered ligands and complexes. As observed for pyrazole-based scorpionates in ref. 46, the B–H stretching vibration appeared to be sensitive to the coordination of the scorpionate ligands to the metal ion. Following the coordination, the B–H band position experienced a shift towards higher wavenumbers by 27–45 cm^{-1} for NO_2-bearing ligands and by 50–56 cm^{-1} in the case of CN derivatives. The high-frequency shift of the B–H stretch is related to the withdrawal of the electron density from the ligand and, consequently, from the boron, upon the coordination. In the IR spectra of the amino-functionalized complexes, the B–H band is located at lower wavenumbers than in the rest of the complexes, *e.g.*, 2474 cm^{-1} for $[Fe(\mathbf{L^5})_2]$ *vs.* 2487 cm^{-1} for $[Fe(\mathbf{L^1})_2]$ and 2470 cm^{-1} for $[Fe(\mathbf{L^6})_2]$ *vs.* 2512 cm^{-1} for $[Fe(\mathbf{L^2})_2]$, which is expected given the electron-

donating effect of the NH_2 group increasing the electron density at boron. An additional characteristic band, positioned away from the rest of the bands, is caused by the stretching vibration of the nitryl group's triple bond inherent in $\mathbf{L^3}$, $\mathbf{L^4}$, **3** and **4**. In these compounds, the band position is situated in a narrow 2245–2251 cm^{-1} range. Unlike the B–H stretching, the position of the C≡N stretching vibration band did not experience any significant shift upon the ligand coordination, though the band is useful for the identification of the respective compounds.

The IR spectra of nitro compounds typically feature the characteristic asymmetric and symmetric stretching vibrations of the NO_2 group. However, they are usually located in the fingerprint region containing a set of other bands that are positioned tightly, which might complicate the assignment of the nitro-group vibrations. Thus, in the spectra of the nitro ligands and their complexes, no bands were found that can be clearly assigned to the NO_2 stretches.

Single crystal and powder X-ray diffraction studies

Single crystals of ^{n}Bu$_4$N$\mathbf{L^1}$ suitable for X-ray diffraction grow in the crude product oily substance in one day. The crystal structure of the heteroscorpionate ligand is shown in Fig. 3. The compound crystallizes in the monoclinic $P2_1/n$ space group, with the desired structure of the heteroscorpionate tetrahedral anion with hydrogen, two pyrazolyl substituents and one 3-nitro-1,2,4-triazolyl function attached to boron as well as tetrabutylammonium as a countercation. Efforts to obtain crystals for the rest of the ligands were not successful.

The crystallization of complexes **1** and **2** by slow evaporation of their saturated solutions or vapor diffusion techniques yielded only polycrystalline aggregates or very small crystals, the quality of which did not meet the requirements for the single crystal X-ray diffraction experiment. Similarly, the endeavor to crystallize complexes **4** and **6** proved unsuccessful. Single crystals of bis[hydrobis(pyrazol-1-yl)(3-amino-1,2,4-triazol-1-yl)]iron(II) (**5**) were grown from a saturated methanolic solution by means of slow evaporation of the solvent. The complex crystallizes in the $P2_1/n$ space group (see Table S1† for crystal data and structural refinement). The coordination environment of Fe^{II} is formed by two coordinated tridentate ligands, the donor atoms of which are resting on the facets of the octahedron. The triazolyl units are located on opposite sides of the axial vertices of the octahedron. Thus, the obtained complex appears in the *trans*-form. Despite the probability of the existence of both *cis*- and *trans*-isomers, only the *trans*-isomer of **5** was observed. The crystal structure of **5** is shown in Fig. 3.

The crystal structure of **5** was acquired at four different temperatures: 100 K, 293 K, 320 K and 393 K. The average distance Fe–N ($\bar{d}_{Fe-N}$) in the complex at 100 K equals 1.986(11) Å, while the octahedron volume (V_p) at this temperature is around 10.46 $Å^3$, which is inherent in low spin iron(II) complexes. The $\bar{d}_{Fe-N}$ value, at room temperature, reaches 2.107(2) Å, which already falls within the range of Fe–N distances found in the HS complexes. At higher temperatures of 320 K and 393 K, the mean iron–nitrogen distances are 2.130(3) Å and 2.159(15) Å, while the polyhedral volume values are 12.80 $Å^3$ and 13.32 $Å^3$, respectively. The octahedron distortion parameter Σ at the termini of the low and high temperature values equals 16.77° and 47.53°, respectively. The unit cell volume (V_c) increases with temperature from 2142.1(10) $Å^3$ (at 100 K) to 2314.06(10) $Å^3$ (at 393 K). Thus, Fe–N distances increase by 8.7% in the full range of temperatures, while the cell volume increases by 8.0%. However, the percentage changes in the thermal evolution parameters should be considered with care, as the thermal expansion in the given temperature range may be non-negligible. The evolution of the structural parameters with temperature for complex **5** is summarized in Table 1 (see detailed crystallographic data in Tables S3 and S4†).

Besides the metal octahedron distortions accompanying the spin crossover, there are also distortions in the ligands. In scorpionate ligands, two main types of distortions in response

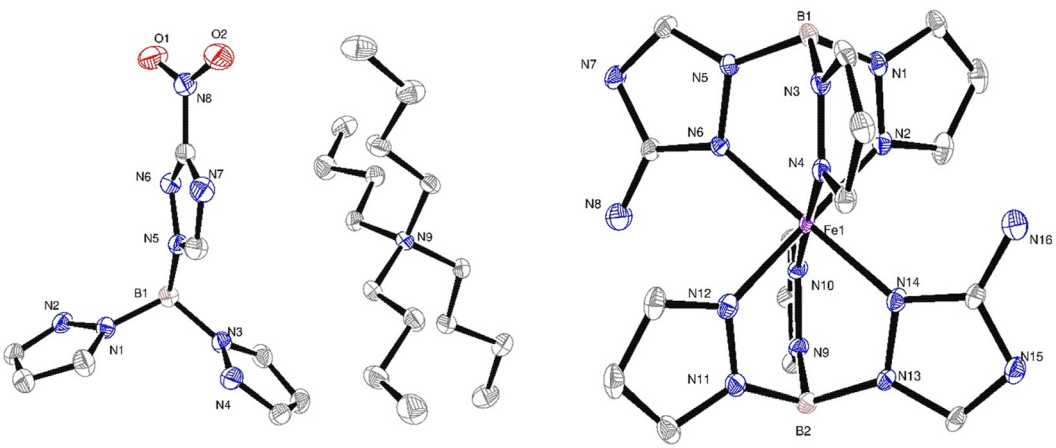

Fig. 3 Crystal structure of ^{n}Bu$_4$N$\mathbf{L^1}$ and complex **5**. Hydrogen atoms, as well as atom labels of carbon and nitrogen of the pyrazolyl fragments, are omitted for clarity. Displacement ellipsoids are drawn at the 50% probability level.

Table 1 Selected structural parameters of **5** at selected temperatures

T, K	$\tilde{d}_{Fe-N}$, Å	Σ, °	V_p, Å^3	V_c, Å^3
100	1.986(11)	16.77	10.46	2142.1(10)
293	2.107(2)	38.59	12.41	2256.1(11)
320	2.130(3)	42.81	12.80	2269.4(2)
393	2.159(15)	47.53	13.32	2314.06(10)

to iron–nitrogen distance increase were established: twisting of a heterocycle ring defined by the B–N–N–Fe torsion angle, and pyramidalization of the boron tetrahedron defined by the distance from boron to the centroid of the B–N-bonded N_3 plane or B–Ct(N_3).[60] These SCO-responsive parameters were measured in coordination compound **5**. It was found that temperature had no considerable effect on the twisting of heterocycle rings. Thus, at 100 K, the triazole rings are twisted to a quite small extent: torsion angles B1–N5–N6–Fe1 and B2–N13–N14–Fe1 are −0.05° and 1.32°, respectively. Meanwhile, at 393 K, these values change to −2.21° and −0.08° respectively. Similar to those for the triazole rings, the B–N–N–Fe torsion angles of the pyrazole changed only by 2.38° maximum. In contrast, the elongation of iron–nitrogen bonds induces pyramidalization of the boron geometry, *i.e.*, a decrease in the distance between boron and the centroid of the mean plane of the boron-bound nitrogen atoms B–Ct(N_3) from 0.57(2) Å at 100 K to 0.522(2) Å at 393 K, which leads to an increase in the ligand bite angle.

Among the interactions determining the crystal packing of [Fe($\mathbf{L}^5$)$_2$] molecules, one can highlight the intermolecular H-bonding between the triazole units formed by a hydrogen atom of the amino group (H-bond donor or D) and the nitrogen atom at position 4 (H-bond acceptor or A) of the heterocycle ring (Fig. 4a). Hydrogen bonding connects the complex molecules in a 1D cascade growing along the *a* crystallographic axis. The distance between hydrogen-bond donors and acceptors d(D···A) is 3.016(3) Å for N8···N15 and 3.012(3) Å for N7···N16 at 100 K. The mean donor–acceptor distance increases by *ca.* 2% at high temperature. Alternatively, C–H···N interactions are present between the triazole and pyrazole units of adjacent [Fe($\mathbf{L}^6$)$_2$] molecules (Fig. 4b). The X-ray diffractogram acquired on the powder of **5** at room temperature matches that simulated from the single crystal diffraction data (Fig. S25†).

Single crystals of complex **3** were obtained by slow evaporation of its saturated DCM solution. The elongated prismatic crystals correspond to the compound that crystallizes in the monoclinic *C*2/*c* space group as a *trans*-isomer (Table S1†). Together with the prismatic crystals, seldom small orthorhombic crystals can be found in the same crystallization batch. These crystals show distinct unit cell parameters and correspond to the *cis*-isomer of the complex that crystallizes as a dichloromethane solvate [*cis*-Fe($\mathbf{L}^4$)$_2$]·CH_2Cl_2 (Fig. 5) in the $P2_1/n$ space group (see detailed crystallographic data in Table S2†). Thus, crystallization of both isomers was observed for complex **3**. However, unlike the case described in ref. 47, no separation of the isomers was achieved by means of column chromatography. Moreover, the PXRD pattern of the same crystallization batch does not contain reflection peaks that might correspond to the *cis*-isomer (Fig. S26†). These observations suggest that the latter may form during the crystallization; however, it is likely a very minor product.

At 100 K, the average Fe–N distance value is 1.976(14) Å in the *trans*- and 1.968(4) Å in the *cis*-isomer. The octahedron volume at the given temperature equals 10.27 Å^3 and 10.16 Å^3 in the *trans*- and *cis*-isomers, respectively. These values indicate that both isomers of the complex are low spin at this temperature. The octahedron distortion of the low-spin *trans*-isomer appears to be higher (19.80°) than that of the LS *cis*-isomer (16.10°). The crystal packing of the isomers is dominated by C–H···N and C–H···π interactions between the complex molecules. The mean D···A distances characterizing the C–H···N interactions in both isomers are 3.424(3) Å in the *trans*- and 3.307(6) Å in the *cis*-isomer. In the case of the C–H···π interactions in the *cis*-isomer, the CH/π-plane distance equals 2.762(4) Å, while the C–H···π access angle is 146.0(4)°, which is in line with typical reported values for such a type of interaction.[61]

Spin crossover properties

The magnetic behavior of the complexes under temperature variation was studied by means of variable-temperature SQUID

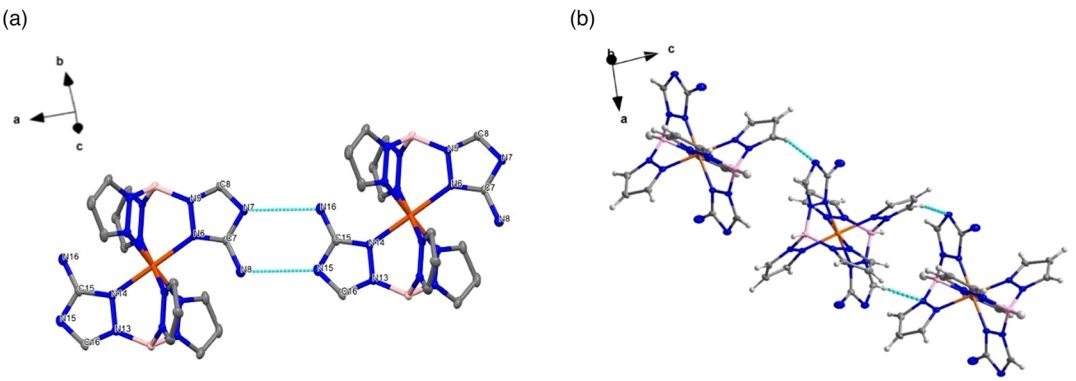

Fig. 4 (a) Hydrogen bonding between [Fe($\mathbf{L}^5$)$_2$] molecules in the crystal of the substance; hydrogen atoms are omitted for clarity. (b) Intermolecular C–H···N interactions between the pyrazole and triazole rings in **5**.

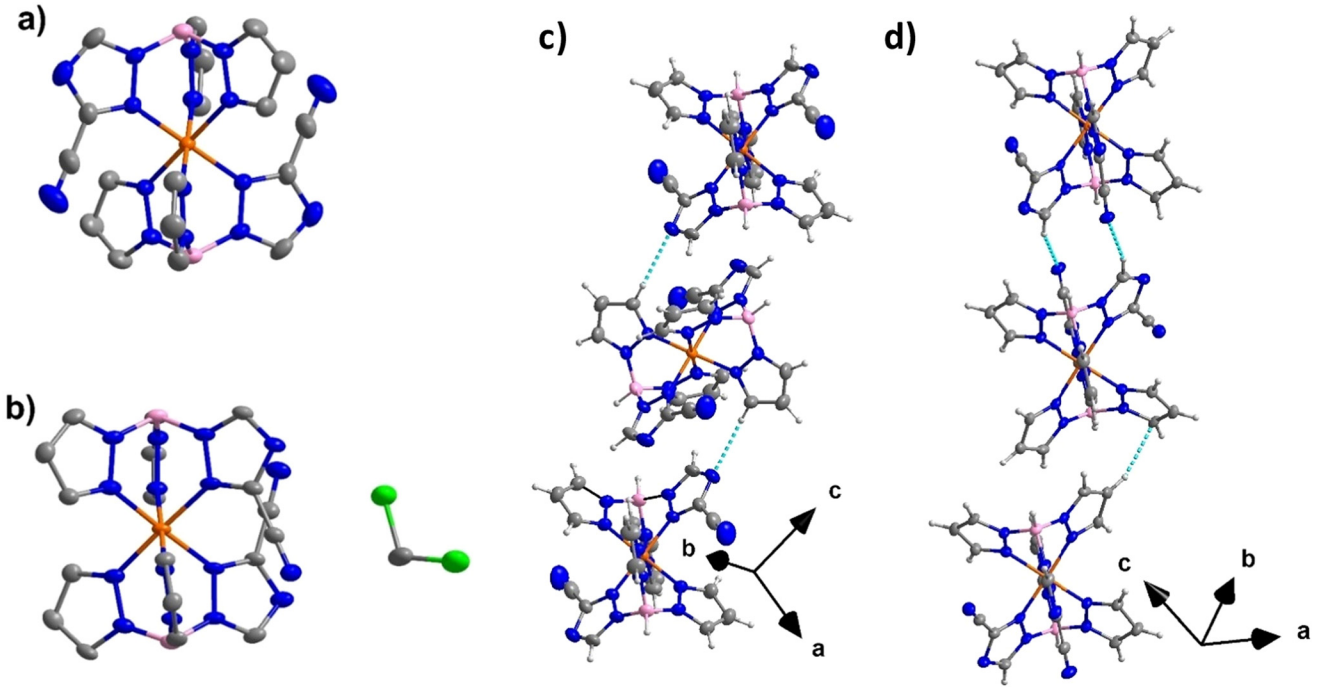

Fig. 5 Crystal structures of the *trans*- (a) and *cis*-isomers (b) of **3**. Hydrogen atoms are omitted for clarity. Displacement ellipsoids are drawn at the 50% probability level. C–H···N intermolecular interactions in the *trans*- (c) and C–H···N together with C–H···π interactions in the *cis*-isomer (d).

magnetometry on bulk powders of the complexes. Molar magnetic susceptibility ($\chi_M T$) was measured in 4–300 K (for **1** and **2**) and 4–400 K (for **3–6**) temperature ranges (Fig. 6). Nitro-functionalized complexes **1** and **2** are high spin at room temperature and retain their HS state at low temperatures until their $\chi_M T$ starts to decrease brusquely below 50 K due mainly to the zero-field splitting. This behavior was also observed for their heteroanalogues containing 3-nitropyrazolyl moieties instead of the nitrotriazole moieties.[46] Referring to the crystallographic data, Ma *et al.* suggested that the effect of the sterically demanding NO_2-substituent situated closely to the metal center allows the ligands to adopt exclusively HS Fe^{II}.

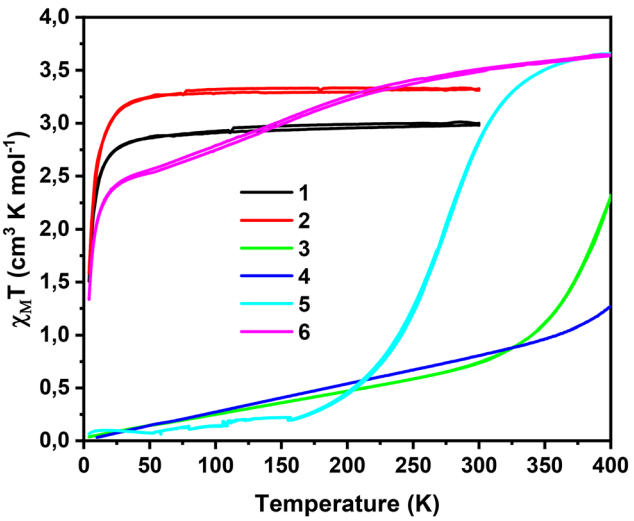

Fig. 6 Molar magnetic susceptibility of **1–6** as a function of temperature in both cooling and heating modes.

Unlike the nitro group, the CN function has no considerable steric effect. Thus, complex **3** bearing two cyano-substituents is low spin at low temperatures, which agrees with the X-ray structural data, and it remains LS at room temperature, whereafter its $\chi_M T$ firmly increases. The transition is not over at 400 K and probably occurs completely at higher temperatures out of the range attainable by the SQUID magnetometry setup used. A similar trend is observed in **4** (tetracyano derivative); however, the threshold of $\chi_M T$ is above 350 K. The amino group is much less bulky compared to the nitro group, and thus the NH_2-substituted ligands are expected to adopt the metal ion in both LS and HS configurations. Indeed, the magnetic measurement data reveal a complete spin transition in diamino-featured complex **5** and incomplete SCO behavior in tetraamino-derived complex **6**. The SCO behavior in the complexes is reproducible over three consecutive thermal cycles. Complex **5** undergoes a gradual spin crossover in the 150–350 K range with $T_{1/2}$ centered around 276 K. The SCO curves of **5** acquired over three consecutive heating/cooling cycles together with the hysteresis loop are shown in Fig. S27.† Despite the presence of hydrogen bonding between $[Fe(\mathbf{L}^5)_2]$ molecules in the bulk of the substance, the SCO occurs gradually. The magnetometry data and the crystallography data correlate well with each other. By comparing the SCO behavior in complex **5** to that of bis[hydrotris(1,2,3-triazol-1-yl)borate]iron(II), one may note that the spin transition in bis[hydrobis(pyrazol-1-yl)(3-amino-1,2,4-triazol-1-yl)]iron(II) is more

gradual. The hydrogen bonding present in the crystal is supposed to favor a more abrupt spin transition. It should be noted however that the H-bonding in the structure is spread only in one dimension, while in previously reported [Fe(HB(1,2,3-tz)$_3$)$_2$] and [Fe(HB(1,2,4-tz)$_3$)$_2$] similar intermolecular C–H···N interactions form 2D and 3D supramolecular networks, respectively, which may promote the cooperativity. Thus, such a gradual SCO behavior in **5** may be explained by the absence of any multidimensional supramolecular network and the lack of other strong intermolecular interactions apart from hydrogen bonding. Besides the structural and magnetochemical characterization, Mössbauer spectra were acquired for the bulk powder of bis[hydrobis(pyrazol-1-yl)(3-amino-1,2,4-triazol-1-yl)] (Fig. S28†). The spectrum acquired at 80 K allows us to conclude that the substance is virtually fully low spin (γ_{HS} = 4%) at this temperature, while at 320 K the HS fraction reaches 94%. Expectedly, γ_{HS} is at equilibrium at 270 K (γ_{HS} = 50%), while at room temperature the compound is 74% high spin. The isomeric shifts, quadrupole splittings, half widths at half maximum (HWHM), acquisition time and high-spin fraction for each temperature are given in Table S5.† The full correlation between the temperature-dependent magnetic susceptibility and Mössbauer spectral data is depicted in Fig. S29.†

The collected structural, magnetochemical and spectroscopic data on the properties of the complexes, when compared to those reported for their 3-nitro- and 3-aminopyrazolyl analogues, can yield some clues on the structure–property relationship. Indeed, iron(II) complexes with heteroscorpionate ligands substituted with bulky NO_2 groups at the 3 position of a heterocycle do not undergo spin crossover as only the HS configuration is sterically favorable for them. Changing the nitro group to the non-bulky CN group affords low spin complexes, which may undergo SCO at high temperatures. Concerning the amino derivatives, one may conclude that replacing the 3-aminopyrazole unit with 3-amino-1,2,4-triazole units makes the HS state more favorable at lower temperatures, thus lowering $T_{1/2}$ or even favoring the incomplete SCO behavior.

Conclusions

Six novel iron(II) coordination complexes incorporating six new heteroscorpionate ligands were synthesized and characterized. SCO behavior (or its absence) in the compounds depended on the steric effect of the substituent (–NO_2, –CN or –NH_2) of the triazole ring at the position proximal to the metal ion. The SCO-active new complexes potentially may provide an extension to the family of thin film thermo-responsive materials. The gradual spin transition in the diamine complex [Fe($\mathbf{L}^5$)$_2$] represents particular interest as it covers cryogenic to above-room-temperature ranges (150–350 K), which is interesting in particular for thermoreflectance-based surface microthermometry applications. Indeed, among the scarce compounds presenting gradual behavior at room temperature (300 K) and without a significant hysteresis loop,[46,62,63] the present compound may represent a unique candidate for sublimation. Thus, future research will concern the assessment of their evaporability and delving into their spin crossover behavior within thin films. This dual focus on SCO phenomena and thermometry highlights the intention to develop advanced materials with tailored characteristics for precise temperature measurement techniques. Moreover, the versatile reactivity of the NH_2 group may allow using amino derivatives as building blocks to extend the family of (evaporable) SCO compounds.

Data availability

The data supporting this article have been included as part of the ESI.†

Conflicts of interest

No conflict of interest.

References

1 *Spin-Crossover Materials: Properties and Applications*, ed. M. A. Halcrow, John Wiley & Sons Ltd, Oxford, UK, 2013.
2 P. Gütlich and H. A. Goodwin, Spin Crossover—An Overall Perspective, in *Spin Crossover in Transition Metal Compounds I*, ed. P. Gütlich and H. A. Goodwin, Springer-Verlag Berlin Heidelberg, Berlin, Heidelberg, 2004, vol. 233, pp. 1–47.
3 A. Bousseksou, Spin Crossover Phenomenon, *C. R. Chim.*, 2018, **21**(12), 1055–1300.
4 M. Cavallini, Status and Perspectives in Thin Films and Patterning of Spin Crossover Compounds, *Phys. Chem. Chem. Phys.*, 2012, **14**(34), 11867.
5 T. Mallah and M. Cavallini, Surfaces, Thin Films and Patterning of Spin Crossover Compounds, *C. R. Chim.*, 2018, **21**(12), 1270–1286, DOI: **10.1016/j.crci.2018.02.007**.
6 H. Soyer, E. Dupart, C. J. Gómez-García, C. Mingotaud and P. Delhaès, First Magnetic Observation of a Spin Crossover in a Langmuir-Blodgett Film, *Adv. Mater.*, 1999, **11**(5), 382–384, DOI: **10.1002/(SICI)1521-4095(199903)11:5<382::AID-ADMA382>3.0.CO;2-U**.
7 O. Roubeau, B. Agricole, R. Clérac and S. Ravaine, Triazole-Based Magnetic Langmuir–Blodgett Films: Paramagnetic to Spin-Crossover Behavior, *J. Phys. Chem. B*, 2004, **108**(39), 15110–15116, DOI: **10.1021/jp048194i**.
8 A. Tissot, J.-F. Bardeau, E. Rivière, F. Brisset and M.-L. Boillot, Thermo- and Photoswitchable Spin-Crossover Nanoparticles of an Iron(II) Complex Trapped in Transparent Silica Thin Films, *Dalton Trans.*, 2010, **39**(33), 7806, DOI: **10.1039/c0dt00321b**.
9 A. Akou, I. A. Gural'skiy, L. Salmon, C. Bartual-Murgui, C. Thibault, C. Vieu, G. Molnár and A. Bousseksou, Soft Lithographic Patterning of Spin Crossover Complexes. Part 2: Stimuli-Responsive Diffraction Grating Properties,

J. Mater. Chem., 2012, **22**(9), 3752–3757, DOI: **10.1039/c2jm15663f**.

10 K. Kuroiwa, T. Shibata, S. Sasaki, M. Ohba, A. Takahara, T. Kunitake and N. Kimizuka, Supramolecular Control of Spin-Crossover Phenomena in Lipophilic Fe(II)-1,2,4-Triazole Complexes, *J. Polym. Sci., Part A: Polym. Chem.*, 2006, **44**(17), 5192–5202.

11 C. Bartual-Murgui, L. Salmon, A. Akou, C. Thibault, G. Molnár, T. Mahfoud, Z. Sekkat, J. A. Real and A. Bousseksou, High Quality Nano-Patterned Thin Films of the Coordination Compound {Fe(Pyrazine)[Pt(CN)$_4$]} Deposited Layer-by-Layer, *New J. Chem.*, 2011, **35**(10), 2089–2094, DOI: **10.1039/c1nj20212j**.

12 S. Cobo, G. Molnár, J. A. Real and A. Bousseksou, Multilayer Sequential Assembly of Thin Films That Display Room-Temperature Spin Crossover with Hysteresis, *Angew. Chem., Int. Ed.*, 2006, **45**(35), 5786–5789.

13 K. S. Kumar and M. Ruben, Sublimable Spin-Crossover Complexes: From Spin-State Switching to Molecular Devices, *Angew. Chem., Int. Ed.*, 2021, **60**(14), 7502–7521.

14 M. Gavara-Edo, F. J. Valverde-Muñoz, R. Córdoba, M. C. Muñoz, J. Herrero-Martín, J. A. Real and E. Coronado, Sublimable Complexes with Spin Switching: Chemical Design, Processing as Thin Films and Integration in Graphene-Based Devices, *J. Mater. Chem. C*, 2023, **11**, 8107–8120.

15 L. Kipgen, M. Bernien, F. Tuczek and W. Kuch, Spin-Crossover Molecules on Surfaces: From Isolated Molecules to Ultrathin Films, *Adv. Mater.*, 2021, **33**(24), 2008141, DOI: **10.1002/adma.202008141**.

16 V. Shalabaeva, S. Rat, M. D. Manrique-Juarez, A.-C. Bas, L. Vendier, L. Salmon, G. Molnár and A. Bousseksou, Vacuum Deposition of High-Quality Thin Films Displaying Spin Transition near Room Temperature, *J. Mater. Chem. C*, 2017, **5**(18), 4419–4425.

17 V. Davesne, M. Gruber, M. Studniarek, W. H. Doh, S. Zafeiratos, L. Joly, F. Sirotti, M. G. Silly, A. B. Gaspar, J. A. Real, G. Schmerber, M. Bowen, W. Weber, S. Boukari, V. Da Costa, J. Arabski, W. Wulfhekel and E. Beaurepaire, Hysteresis and Change of Transition Temperature in Thin Films of Fe{[Me$_2$Pyrz]$_3$BH}$_2$, a New Sublimable Spin-Crossover Molecule, *J. Chem. Phys.*, 2015, **142**(19), 194702, DOI: **10.1063/1.4921309**.

18 M. Gruber, T. Miyamachi, V. Davesne, M. Bowen, S. Boukari, W. Wulfhekel, M. Alouani and E. Beaurepaire, Spin Crossover in Fe(Phen)$_2$(NCS)$_2$ Complexes on Metallic Surfaces, *J. Chem. Phys.*, 2017, **146**(9), 092312, DOI: **10.1063/1.4973511**.

19 O. Iasco, M.-L. Boillot, A. Bellec, R. Guillot, E. Rivière, S. Mazerat, S. Nowak, D. Morineau, A. Brosseau, F. Miserque, V. Repain and T. Mallah, The Disentangling of Hysteretic Spin Transition, Polymorphism and Metastability in Bistable Thin Films Formed by Sublimation of Bis(Scorpionate) Fe(II) Molecules, *J. Mater. Chem. C*, 2017, **5**(42), 11067–11075, DOI: **10.1039/C7TC03276E**.

20 T. Jasper-Tönnies, M. Gruber, S. Karan, H. Jacob, F. Tuczek and R. Berndt, Deposition of a Cationic Fe^{III} Spin-Crossover Complex on Au(111): Impact of the Counter Ion, *J. Phys. Chem. Lett.*, 2017, **8**(7), 1569–1573, DOI: **10.1021/acs.jpclett.7b00457**.

21 A. Mosey, A. S. Dale, G. Hao, A. N'Diaye, P. A. Dowben and R. Cheng, Quantitative Study of the Energy Changes in Voltage-Controlled Spin Crossover Molecular Thin Films, *J. Phys. Chem. Lett.*, 2020, **11**(19), 8231–8237, DOI: **10.1021/acs.jpclett.0c02209**.

22 S. Beniwal, S. Sarkar, F. Baier, B. Weber, P. A. Dowben and A. Enders, Site Selective Adsorption of the Spin Crossover Complex Fe(Phen)$_2$(NCS) on Au(111), *J. Phys.: Condens. Matter*, 2020, **32**(32), 324003, DOI: **10.1088/1361-648X/ab808d**.

23 T. Mahfoud, G. Molnár, S. Cobo, L. Salmon, C. Thibault, C. Vieu, P. Demont and A. Bousseksou, Electrical Properties and Non-Volatile Memory Effect of the [Fe(HB(Pz)$_3$)$_2$] Spin Crossover Complex Integrated in a Microelectrode Device, *Appl. Phys. Lett.*, 2011, **99**(5), 9–11.

24 K. Ridier, A. C. Bas, Y. Zhang, L. Routaboul, L. Salmon, G. Molnár, C. Bergaud and A. Bousseksou, Unprecedented Switching Endurance Affords for High-Resolution Surface Temperature Mapping Using a Spin-Crossover Film, *Nat. Commun.*, 2020, **11**(1), 1–9.

25 O. Y. Horniichuk, K. Ridier, L. Zhang, Y. Zhang, G. Molnar, L. Salmon and A. Bousseksou, *ACS Appl. Mater. Interfaces*, 2022, **14**, 52140–52148.

26 T. Palamarciuc, J. C. Oberg, F. El Hallak, C. F. Hirjibehedin, M. Serri, S. Heutz, J.-F. Létard and P. Rosa, Spin Crossover Materials Evaporated under Clean High Vacuum and Ultra-High Vacuum Conditions: From Thin Films to Single Molecules, *J. Mater. Chem.*, 2012, **22**(19), 9690, DOI: **10.1039/c2jm15094h**.

27 M. Bernien, D. Wiedemann, C. F. Hermanns, A. Krüger, D. Rolf, W. Kroener, P. Müller, A. Grohmann and W. Kuch, Spin Crossover in a Vacuum-Deposited Submonolayer of a Molecular Iron(II) Complex, *J. Phys. Chem. Lett.*, 2012, **3**(23), 3431–3434, DOI: **10.1021/jz3011805**.

28 A. Pronschinske, R. C. Bruce, G. Lewis, Y. Chen, A. Calzolari, M. Buongiorno-Nardelli, D. A. Shultz, W. You and D. B. Dougherty, Iron(II) Spin Crossover Films on Au (111): Scanning Probe Microscopy and Photoelectron Spectroscopy, *Chem. Commun.*, 2013, **49**(89), 10446, DOI: **10.1039/c3cc44904a**.

29 H. Naggert, J. Rudnik, L. Kipgen, M. Bernien, F. Nickel, L. M. Arruda, W. Kuch, C. Näther and F. Tuczek, Vacuum-Evaporable Spin-Crossover Complexes: Physicochemical Properties in the Crystalline Bulk and in Thin Films Deposited from the Gas Phase, *J. Mater. Chem. C*, 2015, **3**(30), 7870–7877.

30 T. G. Gopakumar, M. Bernien, H. Naggert, F. Matino, C. F. Hermanns, A. Bannwarth, S. Mühlenberend, A. Krüger, D. Krüger, F. Nickel, W. Walter, R. Berndt, W. Kuch and F. Tuczek, Spin-Crossover Complex on Au (111): Structural and Electronic Differences Between Mono- and Multilayers, *Chem. – Eur. J.*, 2013, **19**(46), 15702–15709.

31 S. Ossinger, H. Naggert, L. Kipgen, T. Jasper-Toennies, A. Rai, J. Rudnik, F. Nickel, L. M. Arruda, M. Bernien, W. Kuch, R. Berndt and F. Tuczek, Vacuum-Evaporable Spin-Crossover Complexes in Direct Contact with a Solid Surface: Bismuth versus Gold, *J. Phys. Chem. C*, 2017, **121**(2), 1210–1219.

32 S. Rohlf, J. Grunwald, T. Jasper-Toennies, S. Johannsen, F. Diekmann, M. Studniarek, R. Berndt, F. Tuczek, K. Rossnagel and M. Gruber, Influence of Substrate Electronic Properties on the Integrity and Functionality of an Adsorbed Fe(II) Spin-Crossover Compound, *J. Phys. Chem. C*, 2019, **123**(29), 17774–17780.

33 S. Trofimenko, in *Scorpionates: The Coordination Chemistry of Polypyrazolylborate Ligands*, Imperial College Press, London, United Kingdom, 1st edn, 1999.

34 K. Bairagi, A. Bellec, C. Fourmental, O. Iasco, J. Lagoute, C. Chacon, Y. Girard, S. Rousset, F. Choueikani, E. Otero, P. Ohresser, P. Sainctavit, M.-L. Boillot, T. Mallah and V. Repain, Temperature-, Light-, and Soft X-Ray-Induced Spin Crossover in a Single Layer of Fe^{II}-Pyrazolylborate Molecules in Direct Contact with Gold, *J. Phys. Chem. C*, 2018, **122**(1), 727–731, DOI: **10.1021/acs.jpcc.7b11874**.

35 A. Bousseksou, G. Molnár, L. Salmon and W. Nicolazzi, Molecular Spin Crossover Phenomenon: Recent Achievements and Prospects, *Chem. Soc. Rev.*, 2011, **40**(6), 3313.

36 S. Rohlf, M. Gruber, B. M. Flöser, J. Grunwald, S. Jarausch, F. Diekmann, M. Kalläne, T. Jasper-Toennies, A. Buchholz, W. Plass, R. Berndt, F. Tuczek and K. Rossnagel, Light-Induced Spin Crossover in an Fe(II) Low-Spin Complex Enabled by Surface Adsorption, *J. Phys. Chem. Lett.*, 2018, **9**(7), 1491–1496.

37 L. Salmon, G. Molnár, S. Cobo, P. Oulié, M. Etienne, T. Mahfoud, P. Demont, A. Eguchi, H. Watanabe, K. Tanaka and A. Bousseksou, Re-Investigation of the Spin Crossover Phenomenon in the Ferrous Complex [Fe(HB(Pz)$_3$)$_2$], *New J. Chem.*, 2009, **33**(6), 1283.

38 O. Y. Horniichuk, K. Ridier, G. Molnar, V. O. Kotsyubynsky, S. Shova, V. M. Amirkhanov, I. A. Gural'skiy, L. Salmon and A. Bousseksou, *New J. Chem.*, 2022, **46**, 11734.

39 S. Rat, K. Ridier, L. Vendier, G. Molnár, L. Salmon and A. Bousseksou, Solvatomorphism and Structural-Spin Crossover Property Relationship in Bis[Hydrotris(1,2,4-Triazol-1-Yl)Borate]Iron(II), *CrystEngComm*, 2017, **19**(24), 3271–3280.

40 M. D. Manrique-Juarez, F. Mathieu, V. Shalabaeva, J. Cacheux, S. Rat, L. Nicu, T. Leïchlé, L. Salmon, G. Molnár and A. Bousseksou, A Bistable Microelectromechanical System Actuated by Spin-Crossover Molecules, *Angew. Chem., Int. Ed.*, 2017, **56**(28), 8074–8078.

41 V. Shalabaeva, K. Ridier, S. Rat, M. D. Manrique-Juarez, L. Salmon, I. Séguy, A. Rotaru, G. Molnár and A. Bousseksou, Room Temperature Current Modulation in Large Area Electronic Junctions of Spin Crossover Thin Films, *Appl. Phys. Lett.*, 2018, **112**(1), 013301.

42 Y. Zhang, K. Ridier, V. Shalabaeva, I. Séguy, S. Pelloquin, H. Camon, S. Calvez, L. Routaboul, L. Salmon, G. Molnár and A. Bousseksou, A Molecular Spin-Crossover Film Allows for Wavelength Tuning of the Resonance of a Fabry-Perot Cavity, *J. Mater. Chem. C*, 2020, **8**(24), 8007–8011.

43 K. Ridier, Y. Zhang, M. Piedrahita-Bello, C. M. Quintero, L. Salmon, G. Molnár, C. Bergaud and A. Bousseksou, Heat Capacity and Thermal Damping Properties of Spin-Crossover Molecules: A New Look at an Old Topic, *Adv. Mater.*, 2020, **32**(21), 2000987.

44 Y. Zhang, I. Séguy, K. Ridier, V. Shalabaeva, M. Piedrahita-Bello, A. Rotaru, L. Salmon, G. Molnár and A. Bousseksou, Resistance Switching in Large-Area Vertical Junctions of the Molecular Spin Crossover Complex [Fe(HB(Tz)$_3$)$_2$]: ON/OFF Ratios and Device Stability, *J. Phys.: Condens. Matter*, 2020, **32**(21), 214010, DOI: **10.1088/1361-648X/ab741e**.

45 H. Flötotto, T. Secker, P. Kögerler and C. Besson, Amine-Functionalized Spin Crossover Building Blocks, *Eur. J. Inorg. Chem.*, 2019, 4621–4624.

46 C. Ma and C. Besson, Precise Control of the Degree and Regioselectivity of Functionalization in Nitro- and Amino-Functionalized Di(Trispyrazolylborato)Iron(II) Spin Crossover Complexes, *Dalton Trans.*, 2021, **50**(48), 18077–18088.

47 P. J. Desrochers, A. Abdulrahim, K. R. Demaree, J. A. Fortner, J. D. Freeman, M. Provorse Long, M. E. Martin, C. J. Gómez-García and N. Gerasimchuk, Rational Design of Iron Spin-Crossover Complexes Using Heteroscorpionate Chelates, *Inorg. Chem.*, 2022, **61**(47), 18907–18922.

48 G. M. Sheldrick, *Acta Crystallogr., Sect. A: Found. Adv.*, 2015, **71**, 3–8.

49 L. J. Farrugia, *J. Appl. Crystallogr.*, 1999, **32**, 837–838.

50 P. W. Betteridge, J. R. Carruthers, K. Prout and D. J. Watkin, CRYSTALS version 12: software for guided crystal structure analysis, *J. Appl. Crystallogr.*, 2003, **36**, 1487.

51 *International tables for X-ray crystallography*, ed. A. Ibers and W. C. Hamilton, Kynoch Press, Birmingham, England, 1974, vol. IV.

52 L. J. Farrugia, ORTEP3 for Windows, *J. Appl. Crystallogr.*, 1997, **30**, 565.

53 K. Lagarec and D. G. Rancourt, Extended Voigt-Based Analytic Lineshape Method for Determining N-Dimensional Correlated Hyperfine Parameter Distributions in Mössbauer Spectroscopy, *Nucl. Instrum. Methods Phys. Res., Sect. B*, 1997, **129**(2), 266–280.

54 S. Trofimenko, Poly(1-pyrazolyl)Borates, Their Transition-Metal Complexes, and Pyrazaboles, *Inorganic Syntheses*, 1970, vol. 12, pp. 99–109.

55 J. R. Bour, N. M. Camasso and M. S. Sanford, Oxidation of Ni(II) to Ni(IV) with Aryl Electrophiles Enables Ni-Mediated Aryl–CF_3 Coupling, *J. Am. Chem. Soc.*, 2015, **137**(25), 8034–8037.

56 G. Yagil, The Proton Dissociation Constant of Pyrrole, Indole and Related Compounds, *Tetrahedron*, 1967, **23**(6), 2855–2861, DOI: **10.1016/0040-4020(67)85151-2**.

57 E. Radzyminska-Lenarcik, I. Pyszka and W. Urbaniak, New Polymer Inclusion Membranes in the Separation of Palladium, Zinc and Nickel Ions from Aqueous Solutions, *Polymers*, 2021, **13**(9), 1424.
58 J. Sun, Y. Fu, G. He, X. Sun and X. Wang, Catalytic Hydrogenation of Nitrophenols and Nitrotoluenes over a Palladium/Graphene Nanocomposite, *Catal. Sci. Technol.*, 2014, **4**(6), 1742–1748.
59 B. Wrackmeyer and O. L. Tok, Indirect Nuclear Spin-Spin Coupling Constants $^{1}J(^{17}O, ^{11}B)$. First Observation And Calculation Using Density Functional Theory (Dft), *Z. Naturforsch., B: J. Chem. Sci.*, 2006, **61**(8), 949–955, DOI: **10.1515/znb-2006-0804**.
60 D. L. Reger, J. R. Gardinier, J. D. Elgin, M. D. Smith, D. Hautot, G. J. Long and F. Grandjean, Structure-Function Correlations in Iron(II) Tris(Pyrazolyl)Borate Spin-State Crossover Complexes, *Inorg. Chem.*, 2006, **45**(22), 8862–8875, DOI: **10.1021/ic0607437**.
61 M. Nishio, The CH/π Hydrogen Bond in Chemistry. Conformation, Supramolecules, Optical Resolution and Interactions Involving Carbohydrates, *Phys. Chem. Chem. Phys.*, 2011, **13**(31), 13873.
62 C. Rajadurai, F. Schramm, S. Brink, O. Fuhr, M. Ghafari, R. Kruk and M. Ruben, *Inorg. Chem.*, 2006, **45**, 10019–10021.
63 J.-H. Liu, X.-Q. Guo, Z.-C. Wang, L.-X. Cai, L. P. Zhou, C. B. Tian and Q.-F. Sun, *Dalton Trans.*, 2022, **51**, 3894.